Thin Solid Films 518 (2010) 6638–6641

Contents lists available at ScienceDirect

Thin Solid Films

journal homepage: www.elsevier.com/locate/tsf

Bi_2O_3/TiO_2 coaxial nanorods: Synthesis, characterization and photoluminescence properties

C. Hong, H.W. Kim, W.I. Lee, C. Lee *

Department of Materials Science and Engineering, Inha University, 253 Yonghyeon-dong, Incheon 402-751, Republic of Korea

ARTICLE INFO

Available online 12 April 2010

Keywords:
Bi_2O_3-core/TiO_2-shell
Nanorods
Thermal evaporation
Metal organic chemical vapor deposition (MOCVD)
Photoluminescence (PL)

ABSTRACT

Bi_2O_3-core/TiO_2-shell nanorods were prepared by the thermal evaporation of Bi_2O_3 and the metal organic chemical vapor deposition of TiO_2. The Bi_2O_3-core is a pure simple monoclinic α-Bi_2O_3 phase single crystal, whereas the TiO_2 shell has a simple tetragonal structure. The PL emission intensity of the Bi_2O_3 nanorods was enhanced by the TiO_2 coating. The optimal TiO_2 coating layer thickness for the highest emission intensity was 60 nm. On the other hand, the PL properties of the Bi_2O_3-core/TiO_2-shell coaxial nanorods were degraded by post-annealing. The origin of the PL enhancement by the TiO_2 coating is discussed.

1. Introduction

Bismuth oxides have attracted increasing attention owing to their significant energy band gaps (2.85 and 2.58 eV for the monoclinic α-Bi_2O_3 and tetragonal β-Bi_2O_3 phases, respectively), high refractive index, dielectric permittivity, and high oxygen-ion conductivity [1–4], as well as their marked photoconductivity and photoluminescence [5]. These features make the bismuth oxides suitable for sensors, optical coatings, photovoltaic cells, microwave integrated circuits, transparent ceramic glass manufacturing, and cathode ray tubes [6–9]. They are also used in the soft oxidation of hydrocarbons and as electrolyte materials for applications, such as solid oxide fuel cells and oxygen sensors [10,11]. One-dimensional (1D) nanostructures of bismuth oxide are prepared by a range of techniques, such as hydrothermal synthesis [12], microemulsion [13], metal organic chemical vapor deposition [14], atmospheric pressure chemical vapor deposition [15], chemical method [16], oxidative metal vapor transport deposition [17,18], template-based heat treatment [19], thermal oxidation [20], and electrochemical deposition [21]. However, Bi_2O_3 nanorods have not been synthesized by thermal evaporation, which is the simplest and commonest method for the preparation of 1D nanostructures possibly because of the difficulty in their synthesis on silicon substrates.

One-dimensional (1D) nanostructures have been studied extensively on account of their interesting properties and potential applications in electronics and optoelectronics. In particular, coaxial 1D nanostructures with a core/shell geometry have attracted recent attention for two important reasons. One is that the electrical, optical and magnetic properties of materials can be tailored by making 1D coaxial structures [22]. For example, the PL emission intensity of the light emitted from coaxial 1D nanostructures can be increased or the wavelength of the emission can be controlled by selecting a proper coating material and a proper coating layer thickness. The other is to protect the 1D nanostructures from contamination or oxidation and passivation of the abundant interface states at the surface of the 1D nanostructures [23]. This paper reports the successful synthesis of Bi_2O_3-core/TiO_2-shell nanorods on the *c*-plane, i.e. (0001) sapphire substrates. Many materials were attempted as a coating layer for Bi_2O_3, including SiO_2, ZnO, SnO_2, TiO_2, In_2O_3, and Ga_2O_3 thin films. Of these, TiO_2 was found to be the most effective in enhancing the photoluminescence properties of Bi_2O_3 nanowires. The structure and affects of the TiO_2 shell layer thickness and annealing on the photoluminescence properties of Bi_2O_3 nanorods are also reported.

2. Experimental

The preparation of Bi_2O_3-core/TiO_2-shell nanorods consisted of two steps: thermal evaporation of Bi powders in an oxidative atmosphere and MOCVD of TiO_2. First, a gold (Au)-coated sapphire (Al_2O_3 (0001)) substrate was placed on top of an alumina boat containing pure Bi powders positioned at the center of a quartz tube furnace. The furnace was heated to 650 °C and maintained at that temperature under a constant total pressure of 1 Torr with a mixture of nitrogen (N_2) and oxygen (O_2) gas for 1 h. The flow rates of N_2 and O_2 gas were 30 and 5 standard cubic centimeters per minute (sccm), respectively, giving an O_2 partial pressure of 1.5%. The as-grown Bi_2O_3 nanorod samples were then transferred to an MOCVD chamber. The chamber was evacuated to a base pressure of 135 mTorr. Titanium isopropoxide (TTIP) was used as the TiO_2 precursor. N_2 at a flow rate of 30 sccm was used as a carrier gas for TTIP during the coating

* Corresponding author. Tel.: +82 32 7536; fax: +82 32 862 5546.
E-mail address: cmlee@inha.ac.kr (C. Lee).

0040-6090/$ – see front matter © 2010 Elsevier B.V. All rights reserved.
doi:10.1016/j.tsf.2010.03.157

process. At the beginning of the process, oxygen was flushed into the chamber at a flow rate of 2 sccm for approximately 2 s to enhance the dissociation of TTIP. The substrate temperature, canister temperature, and mixture temperature were maintained at 350, 60, and 60 °C, respectively, and the chamber pressure was 800 mTorr throughout the process. The MOCVD process times for the TiO_2 coating were 1–4 h. The Bi_2O_3/TiO_2 coaxial nanorod samples were then annealed at 500 °C for 30 min in an Ar atmosphere.

The morphology and size of the final products were examined by scanning electron microscopy (SEM, Hitachi S-4200). High resolution transmission electron microscopy (HRTEM, Philips CM-200) and selected area electron diffraction (SAED) were carried out at an acceleration voltage of 200 kV. The samples used for characterization were dispersed in absolute ethanol and ultrasonicated before the SEM and TEM observations. The phases of the products were examined by glancing angle (0.5°) X-ray diffraction (XRD). The PL measurements were carried out at room temperature using a He–Cd laser (325 nm) as the excitation source.

3. Results and discussion

Fig. 1(a) and (b) shows typical SEM images of the bismuth oxide (Bi_2O_3) nanorods and TiO_2-coated Bi_2O_3, i.e. Bi_2O_3/TiO_2 coaxial nanorods, synthesized on an Al_2O_3 (0001) substrate, respectively. The Bi_2O_3 nanorods synthesized at 650 °C for 1 h had diameters ranging from 200 nm to 1 μm and lengths ranging from a few tens to a few hundreds of micrometers. The Bi_2O_3-core/TiO_2-shell nanorods prepared by MOCVD of TiO_2 on the Bi_2O_3 nanorods at 100 W for 4 h had diameters of 0.5–1.5 μm. SEM (Fig. 1(a) and (b)) clearly showed that the Bi_2O_3-core/TiO_2-shell nanorods were larger and less uniform in diameter than the Bi_2O_3 nanorods.

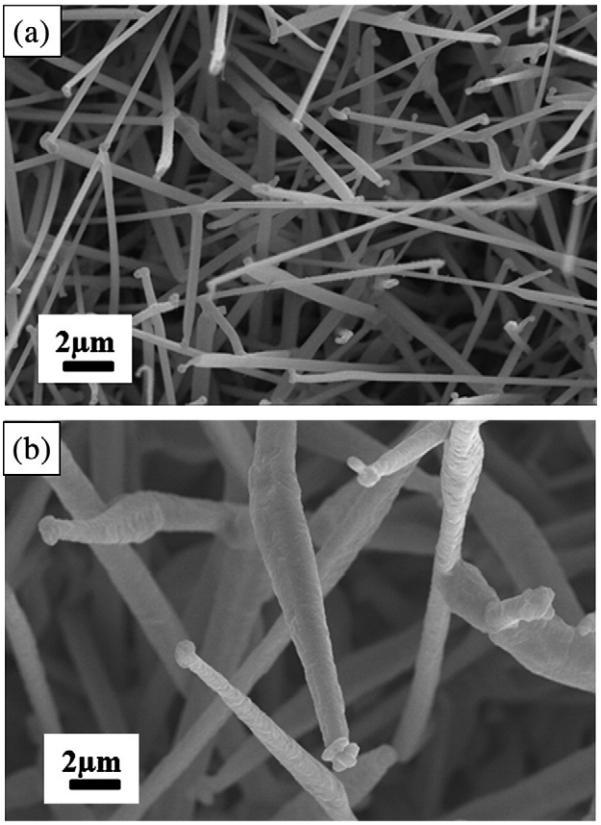

Fig. 1. SEM images of (a) Bi_2O_3 nanorods synthesized by thermal evaporation of Bi powders on Al_2O_3 substrates and (b) the Bi_2O_3-core/TiO_2-shell nanorods prepared by coating the Bi_2O_3 nanorods with TiO_2 by MOCVD at 650 °C for 4 h.

Fig. 2(a) and (b) shows a local HRTEM image and associated SAED pattern of the core/shell interface region, respectively. The TEM image in Fig. 2(a) consisted of two parts: the lower left dark region (the core) and the middle less dark region (the shell). The fringes at the lower left dark region clearly indicate that the Bi_2O_3 core is monocrystalline. In contrast, no clear fringes were observed in the TiO_2 shell at the less dark region. However, a close examination of the associated SAED pattern (Fig. 2(b)) showed that the TiO_2-shells were also crystalline. The SAED pattern recorded perpendicular to the length direction of the nanorod was composed of two sets of spotty patterns: a set with high diffraction intensity for Bi_2O_3 and another with very low intensity overlapped on the Bi_2O_3 pattern. The SAED pattern of the Bi_2O_3 core recorded perpendicular to the length direction of the nanorod corresponds to the [200] zone axis of crystalline α-Bi_2O_3 of a simple monoclinic structure with lattice constants of $a = 0.5849$ nm, $b = 0.8169$ nm, and $c = 0.5631$ nm and an angle between a and c of $\beta = 112.98$. The well defined SAED pattern clearly shows the diffraction spots representing the {200} and {120} lattice planes of α-Bi_2O_3. The interplanar spacings of the core (the upper darker region) were 0.2693 and 0.3255 nm, corresponding to the (200) and (120) crystallographic planes of α-Bi_2O_3. On the other hand, the SAED

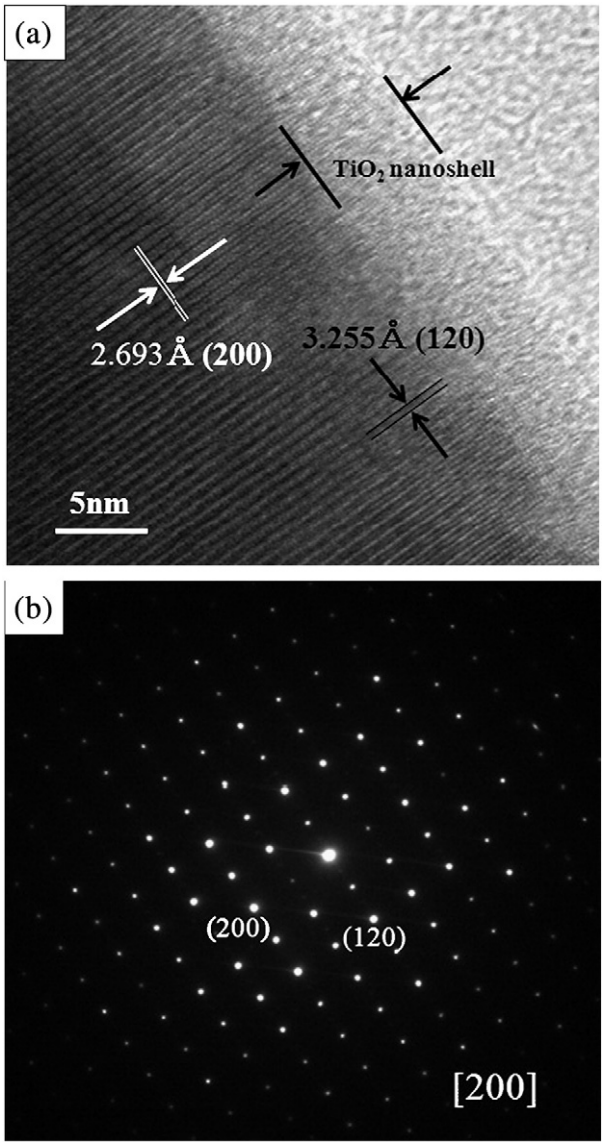

Fig. 2. (a) HRTEM image of a typical Bi_2O_3 nanorod and (b) associated SAED pattern.

pattern of the Bi_2O_3 core must also be a spotty pattern but is too weak to identify its crystal structure.

The structure and phase purity of the Bi_2O_3-core/TiO_2-shell nanorods were examined by XRD. Fig. 3 shows the XRD pattern of the annealed core/shell nanorod samples. All the reflection peaks could be readily indexed to tetragonal α-Bi_2O_3 with lattice constants of $a = 0.5849$ nm, $b = 0.8169$ nm, and $c = 0.5631$ nm (JCPDS 41-1449) and simple tetragonal TiO_2 with lattice constants $a = 0.4593$ nm and $c = 0.2959$ nm (JCPDS 21-1276). No other phase except for α-Bi_2O_3 and TiO_2 was detected in Fig. 3, indicating the high purity of the final products. As is well known, α-Bi_2O_3 is the only low-temperature phase, whereas β-, γ-, and δ- [24] and ω-Bi_2O_3 [25] are high-temperature phases.

Fig. 4 shows change in the PL emission of the Bi_2O_3-core/TiO_2-shell nanorods with an increase in the shell layer thickness. A 325 nm He–Cd laser was used as the excitation source for the PL measurements. The Bi_2O_3 nanorods have a broad emission band centered at approximately 740 nm in the red region. There are no reports of emission at 740 nm, even though there is a report showing broad PL emission bands for Bi_2O_3 nanohook structures at 600–800 nm due to oxygen vacancies [26]. On the other hand, it was reported that TiO_2 nanorods have a broad emission band ranging from 400 to 800 nm with the main peak at approximately 600 nm in the yellow region [27–29].

Fig. 4 suggests that (1) the PL emission intensity of the Bi_2O_3 nanorods can be increased and emission peak shifted to 800 nm by the TiO_2 coating, and (2) the optimum TiO_2 coating layer thickness for the highest emission intensity was found to be 60 nm. There are three possible explanations for the effect of the coating on the PL emission of nanowires by coating: (1) a decrease in the O vacancy concentration in the Bi_2O_3 cores due to the flow of oxygen into the core regions from the atmosphere during the MOCVD process for the TiO_2 shell coating, (2) additional emission from the TiO_2 shell layers, and (3) partial absorption of the light incident upon the nanorods and the light emitted from the cores of the nanorods by the shells on its way in and out. Both the PL enhancing effect due to (1) and (2) and the PL degrading effect due to (3) increase with increasing shell layer thickness. In general, a shift in the emission peak is caused by change in the emission mechanism. It is difficult to say that the shift in the emission peak from 740 nm to 800 nm is attributed simply to the change in the O vacancy concentration in the Bi_2O_3 cores. Since the origin of the PL enhancement is believed to be the same as that of the PL emission peak shift in this nanostructure system, it is possible that emission enhancement does not originate from (1) but from (2). Therefore, the PL enhancement by a TiO_2 coating is due mainly to the additional emission from the TiO_2 shells rather than the increase in emission intensity from the Bi_2O_3 cores. The PL enhancing effect was dominant for the shell layer thickness <60 nm whereas the PL degrading effect was dominant for the shell layer thickness >60 nm. The highest emission intensity of Bi_2O_3-core/TiO_2-shell nanorods appears to be obtained for the shell layer thickness of 60 nm, where the two opposite effects are traded off.

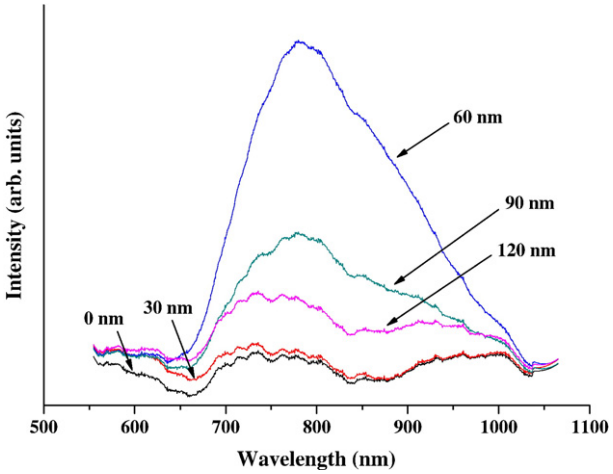

Fig. 4. Photoluminescence spectra of the Bi_2O_3-core/TiO_2-shell nanorods with different shell layer thicknesses.

Fig. 5 shows that the PL property of Bi_2O_3-core/TiO_2-shell nanorods was degraded by annealing regardless of the annealing atmosphere. This degradation might be due to the flow of oxygen from the annealing atmosphere into the Bi_2O_3 cores in the nanorods. EDX spectroscopy analysis was carried out to determine the origin of the degradation. Fig. 6(a) and (b) shows the EDX concentration profiles of Bi, Ti, and O elements along the line drawn across the diameter in the nanorod before and after annealing in an oxygen atmosphere. A comparison of Fig. 6(b) with (a) suggests that a large amount of O atoms flowed into the Bi_2O_3 core during the annealing process, resulting in a decrease in the concentration of oxygen vacancies. As discussed above, the red emission of the Bi_2O_3-core/TiO_2-shell nanorods originates mainly from the deep levels, such as the oxygen vacancies in the Bi_2O_3 cores. Therefore, it is believed that further degradation in the PL emission of the nanorods by oxygen annealing compared to vacuum annealing is caused by the abundant

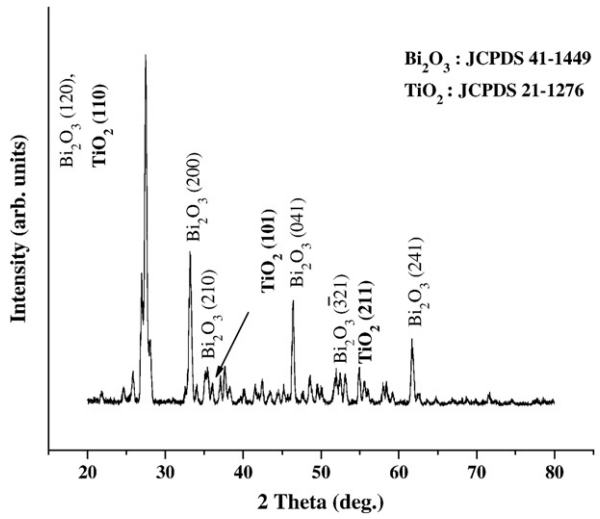

Fig. 3. XRD pattern of the Bi_2O_3-core/TiO_2-shell nanorods synthesized on (0001) Al_2O_3.

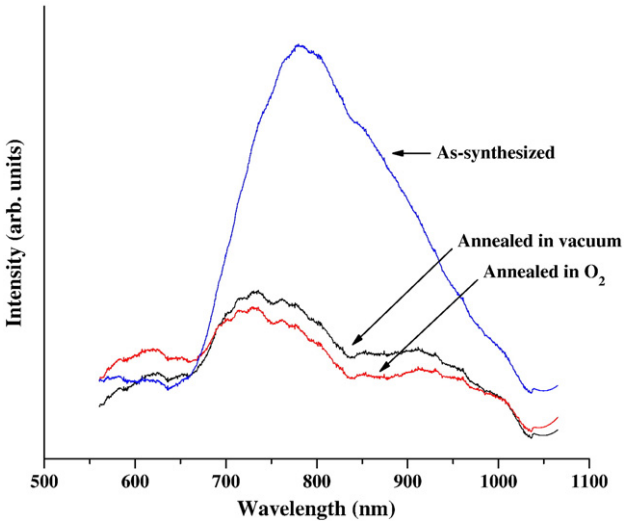

Fig. 5. Photoluminescence spectra of the Bi_2O_3-core/TiO_2-shell nanorods as-prepared and annealed.

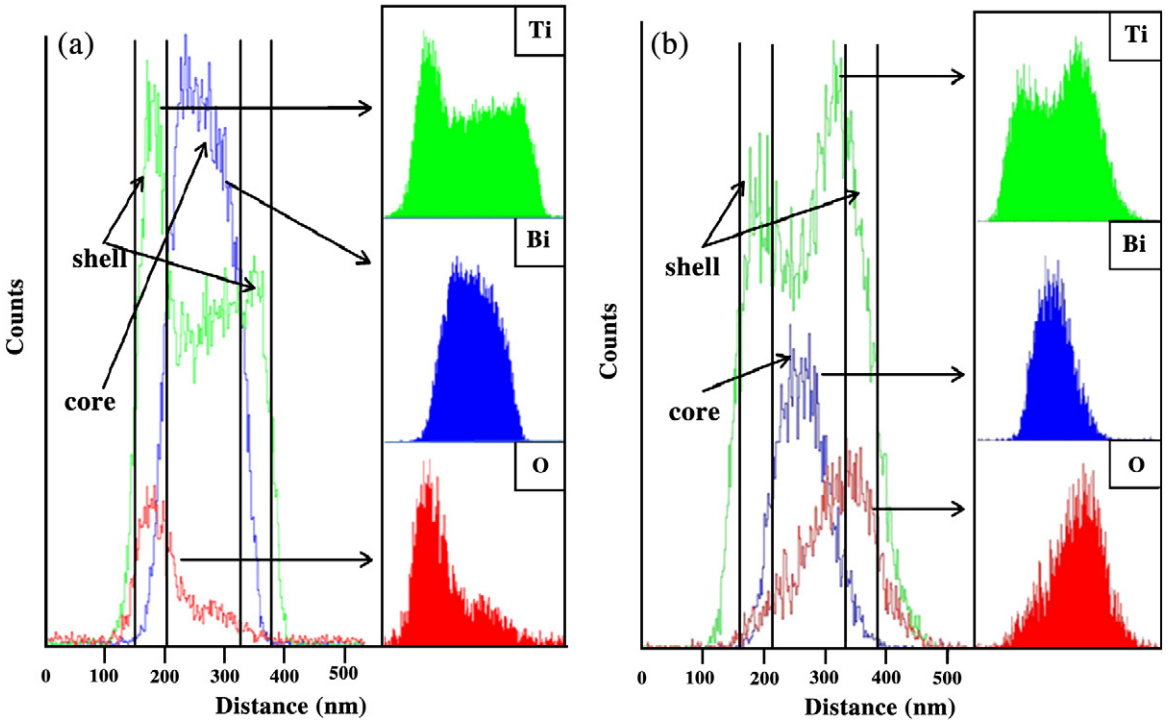

Fig. 6. EDX concentration profiles of Bi, Ti, and O along the diameter of a coaxial nanorod: (a) as-synthesized and (b) annealed in O_2.

supply of oxygen in the annealing atmosphere in addition to the TiO_2 shells.

4. Conclusions

Bi_2O_3-core/TiO_2-shell nanorods were prepared by a two-step process: thermal evaporation of Bi_2O_3 powders and MOCVD of TiO_2. The Bi_2O_3-core is a pure simple monoclinic α-Bi_2O_3 phase single crystal, whereas the TiO_2 shell has a crystalline simple tetragonal structure. Bi_2O_3 nanorods have a broad emission band centered at approximately 760 nm in the red region. The PL emission from the Bi_2O_3 nanorods can be enhanced and shifted to a larger wavelength region by the TiO_2 coating. The optimum TiO_2 coating layer thickness for the highest emission intensity is 60 nm. The PL enhancement by TiO_2 coating was attributed mainly to the additional emission from the TiO_2 shells rather than the increase in emission intensity from the cores. On the other hand, the PL property of the Bi_2O_3-core/TiO_2-shell coaxial nanorods was degraded by post-annealing regardless of the annealing atmosphere due to oxygen flow from the annealing atmosphere to the cores. Further degradation in PL emission of the nanorods by oxygen annealing is caused by the abundant supply of oxygen from the annealing atmosphere and TiO_2 shells.

Acknowledgements

This study was supported by the Korean Science and Engineering Foundation (KOSEF) through the '2007 National Research Laboratory Program'.

References

[1] L. Leontie, M. Caraman, M. Alexe, C. Harnagea, Surf. Sci. 507 (2002) 480.
[2] H. Gobrecht, S. Seeck, H.E. Bergt, A. Martes, K. Kossmann, Phys. Stat. Sol. 33 (1969) 599.
[3] H.T. Fan, X.M. Teng, S.S. Pan, C. Ye, G.H. Li, L.D. Zang, Appl. Phys. Lett. 87 (2005) 231916.
[4] R.L. Thayer, C.A. Randall, S. Trolier, J. Mckinstry, Appl. Phys. 94 (2003) 1941.
[5] N.M. Sammes, G.A. Tomysett, H. Nafe, F. Aldinger, J. Eur. Ceram. Soc. 10 (1999) 1801.
[6] Z.N. Adamian, H.V. Abovian, V.M. Aroutiounian, Sensor Actuat. B 35–36 (1996) 241.
[7] A. Pan, A. Ghosh, J. Non-cryst. solias 271 (2000) 157.
[8] M. Yashima, D. Tshimura, Chem. Phys. Lett. 378 (2003) 395.
[9] E.Y. Wang, K.A. Pandelisev, J. Appl. Phys. 52 (1981) 4818.
[10] M.J. Verkerk, K. Keizer, A.J. Burggraaf, J. Electrochem. Soc. 10 (1980) 81.
[11] N.X. Jiang, E.D. Wachsman, J. Am. Ceram. Soc. 82 (1999) 3054.
[12] Q. Yang, Y. Li, Q. Yin, P. Wang, Y.B. Cheng, Mater. Lett. 55 (2002) 46.
[13] W. Dong, C. Zhu, J. Phys. Chem. Solids 64 (2003) 265.
[14] H.W. Kim, J.H. Myung, S.H. Shim, Solid State Commun. 133 (2006) 177.
[15] X.P. Shen, S.K. Wu, H. Zhao, Q. Liu, Physica E 39 (2007) 133.
[16] T.P. Gujar, V.R. Shinde, C.D. Lokande, S.H. Han, Mater. Sci. Eng. B 133 (2006) 177.
[17] Y. Qiu, D. Liu, J. Yang, S. Yang, Adv. Mater. 18 (2006) 2604.
[18] L. Kumari, J.H. Lin, Y.R. Ma, Nanotechnology 18 (2007) 295605.
[19] B. Yang, M. Mo, H. Hu, C. Li, X. Yang, Q. Li, Y. Qian, Eur. J. Inorg. Chem. 2004 (2004) 1785.
[20] C.C. Huang, K.Z. Fung, Mater. Res. Bull. 41 (2006) 1604.
[21] L. Li, Y.W. Yang, G.H. Li, L.D. Zhang, Small 2 (2006) 548.
[22] L.J. Lauhon, M.S. Gudiksen, D. Wang, C.M. Lieber, Nature 420 (2002) 57.
[23] H.W. Kim, S.H. Shim, C. Lee, Mater. Sci. Eng. B 111 (2004) 131.
[24] S.K. Blower, C. Greaves, Acta Crystallogr. C 44 (1935) 587.
[25] A.F. Gualtieri, S. Immovilli, M. Prudenziatiy, Power Diffract. 12 (1997) 90.
[26] L. Kumari, J.H. Lin, Y.R. Ma, J. Phys. Condens. Matter 19 (2007) 406204.
[27] V.T. Agekyan, Phys. Stat. Sol. A 43 (1977) 11.
[28] S.S. Chang, S.O. Yoon, H.J. Park, Ceram. Int. 31 (2005) 405.
[29] S. Park, C. Hong, J. Kang, N. Cho, C. Lee, Current Appl. Phys. 9 (2009) S230.